

## DIGITAL CLOSE RANGE PHOTOGRAMMETRY FOR MEASUREMENT OF SOIL EROSION

DIRK H. RIEKE-ZAPP (zapp@geo.unibe.ch)  
*University of Bern, Switzerland*

MARK A. NEARING (mnearing@tucson.ars.ag.gov)  
*Southwest Watershed Research Center, Tucson, Arizona, USA*

### *Abstract*

*Many of the processes involved in soil erosion have dimensions on the millimetre scale. Modelling and quantification of such processes require information on soil surface topography with adequate resolution. The purpose of this study was to generate digital elevation models (DEMs) from soil surfaces with high spatial and temporal resolution. Digital photogrammetry was applied for measuring erosion rates on complex-shaped soil surfaces under laboratory rainfall conditions. A total of 60 DEMs were generated, covering a planimetric area of 16 m<sup>2</sup>. The DEMs had a grid resolution of 3 mm. A vertical precision of approximately 1 mm was desired for DEM analysis. A consumer-grade digital camera was used for image acquisition. The camera was calibrated using BLUH software. Homologous points in overlapping images were identified with least squares matching software. Irregularly spaced object coordinates were interpolated to a regular grid in a geographic information system. The resulting DEMs represented the soil surface well. A precision of 1.26 mm in the vertical was attained. The precision of DEM production was limited to camera calibration. Improvements of the setup presented could include the use of better control points and more advanced image matching strategies for identification of homologous points. The DEMs allowed for detailed analysis of soil surface evolution.*

KEYWORDS: digital close range photogrammetry, digital elevation model, soil erosion

### INTRODUCTION

SOIL EROSION is an ubiquitous economic and ecological problem. Detachment and transport of soil particles degrade the fertility of agricultural land and reduce its productivity. Soil erosion causes siltation of ditches and runoff material from eroding surfaces is a major contributor of non-point-source pollutants that accumulate in surface water bodies. Many of the particles involved in soil erosion processes, such as raindrops, soil aggregates, and sediment, have characteristic dimensions on the millimetre scale (Huang, 1998). Modelling and quantification of such processes require detailed information on soil surface topography with adequate resolution and precision (Favis-Mortlock, 1998; Wegmann et al., 2001). Experimental areas for microtopographical studies for soil erosion research range from 1 to approximately 20 m<sup>2</sup>. The grid resolution of digital elevation models (DEMs) for analysis generally varies between 1 and 15 mm (Kuipers, 1957; Elliot et al., 1997; Wegmann et al., 2001; Darboux and Huang, 2003).

Instruments designed for coordinate acquisition typically used by soil scientists range from mechanical point gauges (Kuipers, 1957; Elliot et al., 1997) that make contact with the soil surface, opto-electronic measurement devices (laser scanners) (Römkens et al., 1986; Huang et al., 1988; Darboux and Huang, 2003), and image processing techniques (Welch and Jordan, 1983; Jeschke, 1990; Hancock and Willgoose, 2001; Wegmann et al., 2001; Brasington and Smart, 2003). Point gauges were widely replaced by laser scanners because the former make contact with the soil and can thus disturb it or sink into it. While laser scanners have proven their usefulness in many experiments, a photogrammetric system allows for more rapid data acquisition on the job, employs a more flexible camera-to-object distance, and ultimately allows for a wider vertical range of the DEM. In addition to that, a camera is easier to handle, and a photogrammetric system can be scaled according to the project requirements (Rieke-Zapp et al., 2001).

Analytical photogrammetry has often been used for geomorphological studies (Welch and Jordan, 1983; Kirby, 1991; Merel and Farres, 1998; Clegg et al., 1999). Automated digital photogrammetry allows DEMs to be generated with sufficient resolution for microtopography analysis. Jeschke (1990) applied correlation matching to soft copy images of a Zeiss SMK 40 for analysis of soil microtopography. Recent advances in digital image processing and camera calibration techniques allow the use of digitised images taken with consumer-grade analogue cameras for automated DEM generation (Stojic et al., 1998; Hancock and Willgoose, 2001; Brasington and Smart, 2003). Pyle et al. (1997), Rieke-Zapp et al. (2001), Wegmann et al. (2001), Chandler et al. (2002), as well as Lascelles et al. (2002) calibrated consumer-grade cameras and employed the imagery for automatic DEM generation in digital photogrammetric workstations, which are becoming increasingly accessible to non-photogrammetrists.

The purpose of this experiment was to develop a method for measuring erosion rates and rill network evolution on complex-shaped soil surfaces under laboratory rainfall simulation conditions. A rainfall experiment was designed in a  $4 \times 4 \times 0.8 \text{ m}^3$  flume (Fig. 1) to study the effect of slope shape on soil erosion during rainfall experiments. DEMs with a resolution of 3 mm on the ground and a precision of approximately 1 mm in all dimensions were desired for

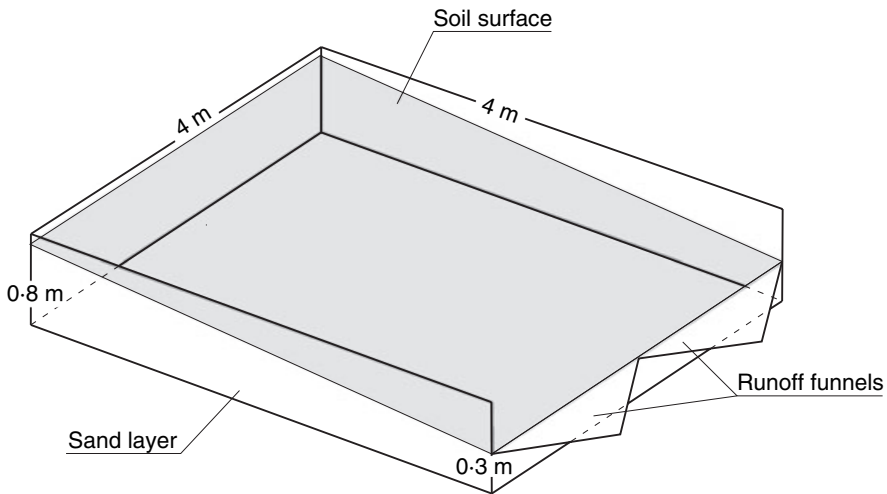


FIG. 1. The experimental flume with dimensions of  $4 \times 4 \times 0.8 \text{ m}^3$ . A 0.2 m thick soil layer was prepared on a sand layer. Runoff and sediment yield were collected at the two flume outlets. Rainfall simulators were placed approximately 3.7 m above the flume.

analysis. Preparation of different slope shapes resulted in large vertical deviations of as much as 0.4 m in the soil surface elevation from the tilted plane, and hence laser technology was not applicable in this case. Also, the experiment required that the soil surface remain undisturbed, and therefore only a non-contact survey technique was feasible. Photogrammetry was also preferred over laser scanning since it allowed more rapid data acquisition and because it was capable of producing DEMs with the desired resolution and precision.

Photogrammetric hardware and software were acquired to generate soil surface DEMs according to the outline of the project. A system leaving most control to the user was preferred (Rieke-Zapp et al., 2001; Wegmann et al., 2001) over an automated system where the user has little control over decisions taken by the software (Stojic et al., 1998; Chandler et al., 2002; Brasington and Smart, 2003). While the latter solution requires less expert knowledge in photogrammetry and is more user friendly, the users have little control over camera calibration, image correlation parameters or interpolation and smoothing of the DEM. An additional requirement for the system was that the software should run on a personal computer. Experiences in obtaining the desired erosion and topographic information, as well as advantages and disadvantages of the photogrammetric system used, will be presented and discussed in this paper.

#### RAINFALL SIMULATION EXPERIMENT

A rainfall study was prepared in a wooden box with dimensions of  $4 \times 4 \times 0.8 \text{ m}^3$ , length, width, and height, respectively (Fig. 1). The bottom part of the box was filled with silica sand to allow free drainage. The sand was covered with soil that was taken from the top 0.4 m of a "Typic Hapludalf" common in the area of West Lafayette, Indiana, USA. It contained  $50 \text{ g kg}^{-1}$  sand,  $720 \text{ g kg}^{-1}$  silt, and  $230 \text{ g kg}^{-1}$  clay. The organic matter content was  $20 \text{ g kg}^{-1}$ . The soil was sieved to pass through an 8 mm grid and was loosely packed in the box. Soil depth in the flume was at least 0.2 m above the silica sand layer. Total soil depth varied for different slope shapes. Four rainfall simulator troughs, each with four V-Jet nozzles, were raised approximately 3.7 m above the soil surface. The soil surface was pre-wetted several times with low intensity rainfall that produced only minimal amounts of runoff over a period of 5 days before the experiment. Both water and sediment samples were collected at the flume outlets at 1 to 2 min intervals during the experiments. Images for DEM generation were acquired before the experiment and after 10, 20, 40, 60, and 90 min of the experiment with the rainfall stopped. The time required for data acquisition was 20 min after the rainfall stopped, including a 10 min waiting period to drain excess water from the wet soil surface that could cause reflections. This time was used to bring the camera into position and to wipe control points around the flume clear from water and sediment.

#### THE CAMERA SYSTEM

A Kodak DCS1 monochrome digital camera was used to capture images for DEM generation. The camera is composed of two parts: (i) a Canon EOS 1N camera body and (ii) a digital camera back with a charge-coupled device (CCD) sensor fitted to the camera body. The digital back also housed the battery and the Personal Computer Memory Card International Association (PCMCIA) card drive to save image files. Camera and digital back were held together by a single screw. The camera design is very similar to the more commonly used Kodak DCS460m that uses the same image sensor, but is integrated in the Nikon photo system. Forkert and Stanek (1997) have shown that the position of the principal point inside a similar Kodak camera was changed by approximately 20 pixels just by turning the camera upside

down. Similar problems were reported by Gruen et al. (1995) as well as Peipe and Schneider (2003). Therefore, to stabilise the sensor inside the camera, the CCD chip was removed from the digital back and fixed in the film plane of the camera body. This mechanical fixation of the chip was favoured over the use of image variable parameters of interior orientation for camera calibration (Gruen et al., 1995; Maas, 1999; Tecklenburg and Luhmann, 2001). The CCD sensor had a matrix of  $3060 \times 2036$  picture elements (pixels). The distance between two pixel centres was 0.009 mm. The sensor was 1.3 times smaller than the 35 mm film format. The Kodak DCS1m was the only digital camera at the time of camera acquisition that allowed mirror lock-up. This feature reduced image blur due to vibrations caused by mirror slap that becomes visible in the images at longer shutter speeds.

Using a monochrome camera has several advantages over a digital camera with red-green-blue (RGB) colour sensor as was used in similar previous studies (Lascelles et al., 2002; Brasington and Smart, 2003). A monochrome sensor has no colour filter in front of the sensor. This increases the International Organization for Standardization (ISO) rating of the sensor to 200 as compared to ISO 80 for the colour version of the same sensor. All pixels are sensitive to the same spectrum of light. The information at each pixel location is not interpolated on a monochrome sensor. Pixels of a typical RGB colour sensor are arranged in a one layer matrix of which 50%, 25%, and 25% are masked green, red, and blue, respectively. During post-processing this single layer of pixels is interpolated to a triplet of layers, meaning that 50%, 75%, and 75% of the pixels representing the green, red, and blue channels of the image, respectively, must be interpolated from pixels with a different colour. This interpolation can lead to artefacts in the images, reducing the geometric quality of the image. Saving the three layers in separate colour channels triples the size of one image to 18 MB for a sensor with 6 million pixels and 8 Bit colour depth, as compared to a monochrome image, while no information is added. Image correlation software typically employs only one colour channel of an image for analysis (DPCOR, 2000; ERDAS, 2002). This implies that 100% of the original information of a monochrome sensor can be utilised by the software while a single layer of a colour image will carry at most only 50% of the original resolution of an RGB sensor. At the same time, image file size is reduced and light sensitivity of the sensor is increased when using a monochrome camera. An image size of 6 MB allowed analysis to be performed on uncompressed Tagged Image File Format (.TIFF) images.

The camera only accepted Canon EF mount lenses. These autofocus lenses are designed for quick focusing with low resistance for the focusing engine. As a result, the position of the lens elements is typically not as stable as for manual focus lenses resulting in unstable camera geometry. To avoid this problem, a Leica R 2.8/19 mm lens and a Schneider 2.8/28 mm lens were fitted to the Canon EF mount. Both lenses are manual focus lenses with stable mechanics and superior image quality. Tests have shown that the resolving power of both lenses was sufficient to capture object detail over the whole image frame, which is not necessarily true for all lenses offered for a specific camera mount. This is particularly true when image sensors near to the full 35 mm format are used that require best optical performance for a large image circle (Peipe and Schneider, 2003). Metal rings were fitted around the focusing rings of the lenses to fix specific distances for which the camera could be calibrated (Fig. 2).

## IMAGE ACQUISITION

The Kodak camera was used in combination with the 19 mm lens to capture the soil surface with overlapping imagery (Table I; Fig. 3). The 19 mm lens with the wider field of view was chosen due to the limited distance between soil surface and rainfall simulators. Optimum image quality was accomplished with the aperture set to  $f/9.5$ , the exposure time



FIG. 2. Kodak DCS1m with Leica 19 mm lens mounted and Schneider 28 mm lens in the foreground. Images are saved on PCMCIA cards. Metal rings were fitted around both lenses to fix the focus distance and allow calibration for different reproducible distance settings.

set to 0.17 s, and mirror lock-up. The aperture setting resulted in a depth of field from approximately 0.6 m to infinity. This was of great advantage when taking oblique images of the flume for camera calibration. Two strips of images were required to cover the flume with adequate resolution and to minimise the amount of obstructed areas due to deep and narrow rills that formed on the soil surface during the experiments. The camera was positioned along a metal beam supported by A-frames at both ends. The camera was moved along a line that was parallel to the general slope of the soil surface. The shutter was controlled with a cable release. Image acquisition for the entire plot took approximately 5 min. Raw image data was captured on PCMCIA drives and transferred to a desktop computer for analysis.

Ground control points were placed around the flume. The soil surface was kept free of control points. Therefore, surface water flow, raindrop impact, and other erosion processes remained unaffected. Control points were marked as white ellipses on a black background. A centre of gravity operator in DPLX (2000) software was used to identify the targets with sub-pixel precision in image space. Control points were laminated to make them resistant to water and dust. An independent survey of ground control points was not feasible due to space

TABLE I. Flight planning details for stereo coverage of the soil box.

<i>Parameter</i>	<i>Values</i>
Image size	27·540 mm × 18·324 mm
Pixel size	0·009 mm × 0·009 mm
Focal length ( <i>c</i> )	19 mm
Area of stereo coverage	4500 mm × 4500 mm
Ground sample distance	0·9 mm pixel <sup>-1</sup>
Image scale (m)	1:100
Height above surface ( <i>h</i> )	1900 mm
Base length ( <i>b</i> )	733 mm
Height to base ratio ( <i>h/b</i> )	2·59
Forward overlap of images	60%
Sidelap	30%
Number of image strips	2
Number of images in one strip	7
Additional images for block stability	2
Total number of images per block	16

limitations around the flume. The coordinates of the control points were determined photogrammetrically during camera calibration. Tie points were measured in all images for DEM generation to increase the geometric stability of the block (Fig. 3).

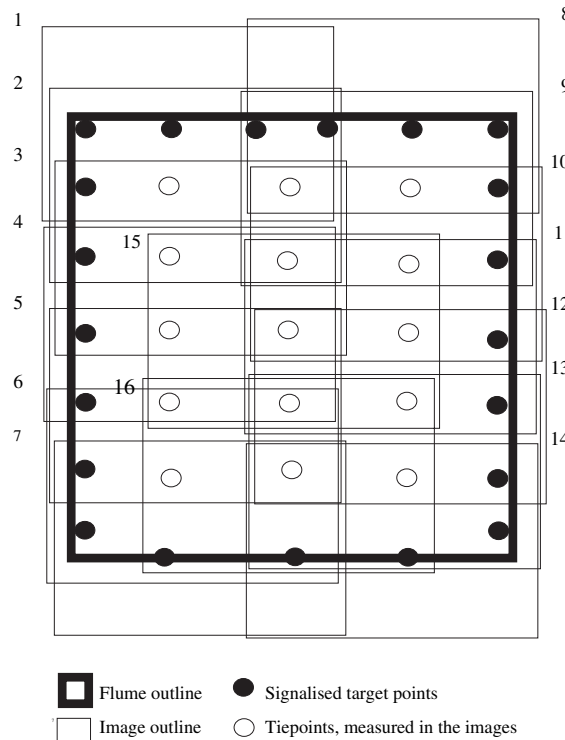


FIG. 3. Arrangement of images for stereo coverage of the flume. Each point symbol represents a cluster of points. Images 15 and 16 were used to increase block stability in the centre of the flume.

## CAMERA CALIBRATION

The Kodak camera is a non-metric camera that requires calibration with the lens before it can be used for precise photogrammetric measurements. The camera was calibrated with BLUH software (Jacobsen, 1980, 2000). BLUH is commercial bundle block adjustment software that allows camera calibration of the interior orientation plus up to 12 additional parameters for cameras of this type. Statistical tests were performed, using the software to test for significance of additional parameters and for identification of blunders in the data set. The additional BLUH parameters 1 to 12 were found to be significant in order to account for radial symmetric lens distortion as well as other systematic deviations of the camera geometry from the frame camera model. The camera was calibrated prior to each experiment (Table II).

All coordinates were referenced to a testfield with dimensions of  $2150 \times 1460 \times 350 \text{ mm}^3$ . The testfield was placed on timber logs in the centre of the flume prior to the experiment (Fig. 4). Control points on the testfield were measured with an accuracy of 0.2 mm in all dimensions using a coordinate measurement machine at Subaru Isuzu Automotive (SIA), West Lafayette, Indiana, USA. Additional targets were placed on the timber logs in order to fill the entire image frame with targets signalised in object space. Approximately 20 images were taken for calibration with the testfield in the centre of the flume. The camera was aimed at the flume from different directions to create a robust network of measurements for the bundle block adjustment. In addition, the camera was rolled about the optical axis between image acquisitions to reduce statistical correlation of parameters used to model the interior geometry of the camera (Wester-Ebbinghaus, 1985; Godding, 1993).

All images taken for calibration, as well as the images taken for DEM generation, were introduced in a single bundle block adjustment. This procedure ensured the best relative orientation of all images as well as a large redundancy of the adjustment. Testfield coordinates were not fixed in the adjustment, but introduced with their calibrated accuracy. Therefore, the results of the bundle block adjustment (Table II) are only valid as estimates of the internal precision of the adjustment, and no conclusions can be drawn about the accuracy in object space. To check if the precision of the bundle block adjustment can be attributed to a length in object space, the calibrated length of a scale bar, which was not introduced as an observation in the adjustment, was compared to the calculated distance between two targets placed on the scale bar (Table III).

TABLE II. Typical results of the bundle block adjustment with BLUH using the Kodak DCS1m camera with a 19 mm lens including camera calibration with 12 additional parameters that were identified to be significant by the software.

<i>Image space parameter</i>	<i>Value (mm)</i>	<i>Standard error (mm)</i>	<i>Standard error (pixel)<sup>a</sup></i>
Focal length	18.8557	±0.0018	±0.20
Shift to PP <sup>b</sup> in <i>x</i>	-0.3684	±0.0011	±0.12
Shift to PP <sup>b</sup> in <i>y</i>	-0.3480	±0.0014	±0.16
<i>Object space</i>	<i>X (mm)</i>	<i>Y (mm)</i>	<i>Z (mm)</i>
RMSE of differences at control points	0.031	0.042	0.069
<i>A posteriori</i> $\sigma_0$			
0.0020 mm or 0.22 pixel			

<sup>a</sup>The dimension of one pixel is 0.009 mm.

<sup>b</sup>Principal point.

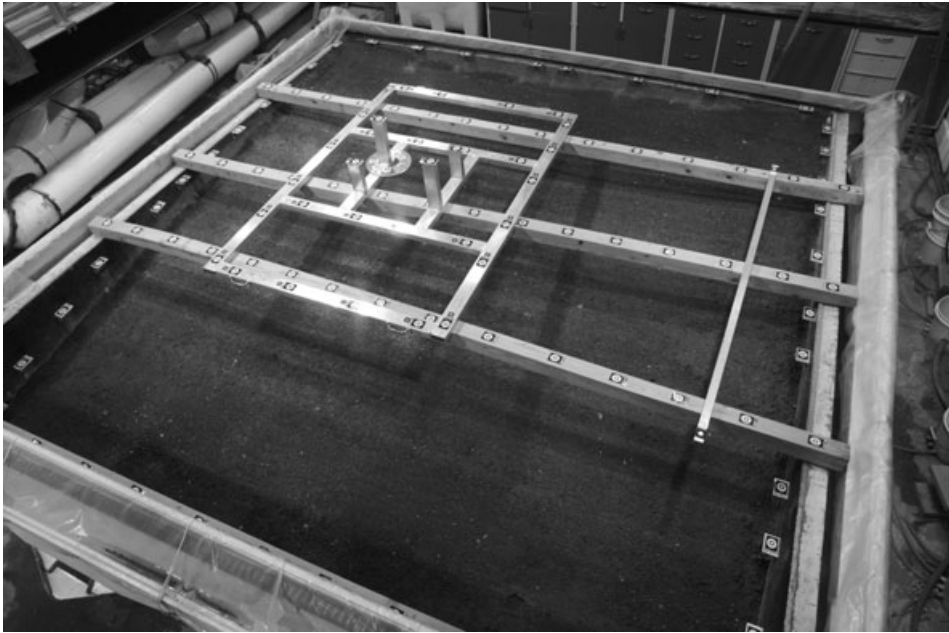


FIG. 4. A testfield was positioned on timber logs in the centre of the flume when taking images for camera calibration. In addition, a scale bar was placed in one part of the flume for control of the precision estimates resulting from the bundle block adjustment for self-calibration.

The distance between the targets on the scale bar was also calibrated at SIA with an accuracy of 0.2 mm. The scale bar was placed at the corner of the flume to check if the extrapolation of testfield coordinates over the area of the flume led to a systematic decrease of precision away from the testfield. In 10 experiments the length calculated from the bundle block adjustment for self-calibration always fell short of the calibrated length. The Root Mean Square Error (RMSE) was calculated from the deviations of the 10 experiments (Table III). Values indicated that sub-millimetre accuracy was accomplished for coordinates, while relative precision of the coordinates was estimated even better. The systematic underprediction of the

TABLE III. Scale bar calibration of the camera.

<i>Calculated length of scale bar (mm)</i>	<i>Deviation from reference length (mm)</i>
2003-697	-0.020
2003-517	-0.200
2003-328	-0.389
2003-527	-0.190
2003-453	-0.264
2003-544	-0.173
2003-695	-0.022
2003-434	-0.283
2003-417	-0.300
2003-682	-0.035
Calibrated length: 2003-717	RMSE = 0.235

calibrated scale bar length might be attributed to extrapolation of object coordinates from the centre of the flume towards the edges. The absolute deviation of approximately 0.2 mm is negligible for this experiment.

In addition to the scale bar check, distances between control points across the flume were measured with a tape measure and compared with the distances calculated in the bundle block adjustment.

The typical amount of data processed in the bundle block adjustment for one experiment included approximately 120 images, and 7000 observations to solve for 2000 unknowns. Unknowns were the interior orientation of the camera including additional parameters, the exterior orientation of the images, as well as the object coordinates of all measured points, including control and tie points. Errors in the data set were identified in BLUH and corrected or excluded from the adjustment.

### DEM GENERATION

After restitution of image and camera orientation, homologous points in overlapping images were identified with DPCOR (2000) software. DPCOR applies correlation-based matching techniques for automatic detection of homologous points. The software was developed to work in imagery with unknown orientation and does not require or apply any information regarding exterior or interior orientation, such as epipolar lines as are used in ERDAS IMAGINE OrthoBASE (ERDAS, 2002) or the vertical line locus strategy used in LISA (Linder, 2003). DPCOR applies the algorithm of Gruen (1985, 2001) for least squares matching in image space. The grey values of a matrix of pixels in one image (the reference scene) are compared to a matrix of pixels in a second image (the search scene). The search matrix is geometrically and radiometrically adjusted and the cross-correlation coefficient between the matrices in both images is calculated. The geometric correction is based on a six-parameter affine transformation with two shift, two scale, and two shear parameters. DPCOR includes error-checking routines and the user can set limits to all parameters that are involved in the matching process (Table IV).

Least squares matching allows for sub-pixel precision of matches in image space. Candidates for homologous points are identified using the region-growing algorithm (Otto and Chau, 1989). The user provides starting points (seed points) that are used as an approximation for the matching process. After matching the seed points, the program will apply the region-growing algorithm to identify homologous points in the search scene that correspond to a regular grid of points in the reference scene. The density of the grid in the reference scene and

TABLE IV. Parameters and limits for matching of homologous points with DPCOR software. Pooled RMSE values are calculated from 12 samples with more than 1 million matched points.

<i>Parameter</i>	<i>Value</i>
Matching window size (pixel)	11 × 11
Max. number of iterations	7
Step size in row and column direction (pixel)	2
Max. difference from initial position (pixel)	5
Acceptance bound for correlation coefficient	0.8
Min./max. bound for scale parameters	0.5/2.0
Min./max. bound for rotation and shear parameter	-0.8/0.8
RMSE of shift parameters (row/column) (pixel)	0.027/0.017
RMSE of shift parameters (row/column) (mm <sup>a</sup> )	0.00024/0.00015

<sup>a</sup>The dimension of one pixel is 0.009 mm.

therefore the number of possible matches is defined by the user (step size, Table IV). Information from successfully matched seed points will be used to approximate the position of neighbouring matching candidates in the search scene. After matching a homologous point in the search scene, the software attempts to match the four immediate grid neighbours of the point. This means that each successfully matched point will generate up to four new candidates to continue region growing. The correlation coefficient is the most important indicator for matching success. Therefore, region growing will continue from the successfully matched point that had the largest correlation coefficient. The list of successful matches grows with the progress of region growing in the program. The greater the number of points that were successfully matched, the more time was needed to loop through the list to identify the next best candidate for matching. This process becomes increasingly demanding on the central processing unit (CPU) of the computer, resulting in an exponential increase in computing time as a function of the number of possible or attempted matches. The standard deviation of the shift parameters can be used as an estimate of the precision of the matching in image space. Sub-pixel precision was accomplished for all matches (Table IV).

Object coordinates were calculated from the homologous points by spatial intersection in BLUH software. DPCOR software did well avoiding mismatches; however, areas with low contrast, areas with large relief displacement, areas obstructed in one of the images, or areas with surface discontinuities (such as rills) lead to mismatches with an offset of several pixels in image space, while the correlation coefficient and the precision estimates of the match would reflect a successful match. This problem can be attributed in part to the fact that DPCOR does not apply any matching constraints based on camera geometry or image orientation. Therefore, only matches with a relatively large correlation coefficient of 0.8 were accepted, while, for instance, Stojic et al. (1998) and Linder (2003) worked with a correlation coefficient limit of 0.6 when including epipolar geometry or vertical line locus constraints. Still, some mismatches could be identified in the data set matched with DPCOR. Those were reduced by applying a parallax limit of 1 mm for spatial intersection for object coordinate generation in BLUH software. This constraint helped to minimise the number of object coordinates with low precision before DEM interpolation that resulted from mismatches or from low precision of camera calibration that was visible in the corners of the images.

After calculation of object coordinates, point clouds of irregularly spaced object coordinates were interpolated to regular grids (DEMs). Inverse distance weighted (IDW) interpolation with four neighbours and a power factor of two was used in ArcView 3.2a GIS for interpolation of DEMs with 3 mm cell size. This interpolation method minimised the amount of smoothing during DEM generation.

## RESULTS AND DISCUSSION

A total of 60 DEMs were generated. The equipment allowed quick data acquisition on the job, did not disturb the soil surface, and produced DEMs that could be used for subsequent erosion and morphological change analysis. The DEMs were visually inspected and compared to the images, which serve as a permanent record of the surface. Visually, the DEMs represented the soil surface well, showing most of the detail visible in the images (Fig. 5). Application of rigorous constraints during the matching process led to successful matching of approximately 80% of all possible matches per stereopair. The relatively continuous soil surface was well suited for the matching with DPCOR. The 20% of missing matches were due to obstructed areas in the images that are not visible in both scenes and to areas where object contrast was too low to allow successful matches. In some instances water ponded on the surface made matching impossible since the drops reflected light differently depending on the position of the camera.

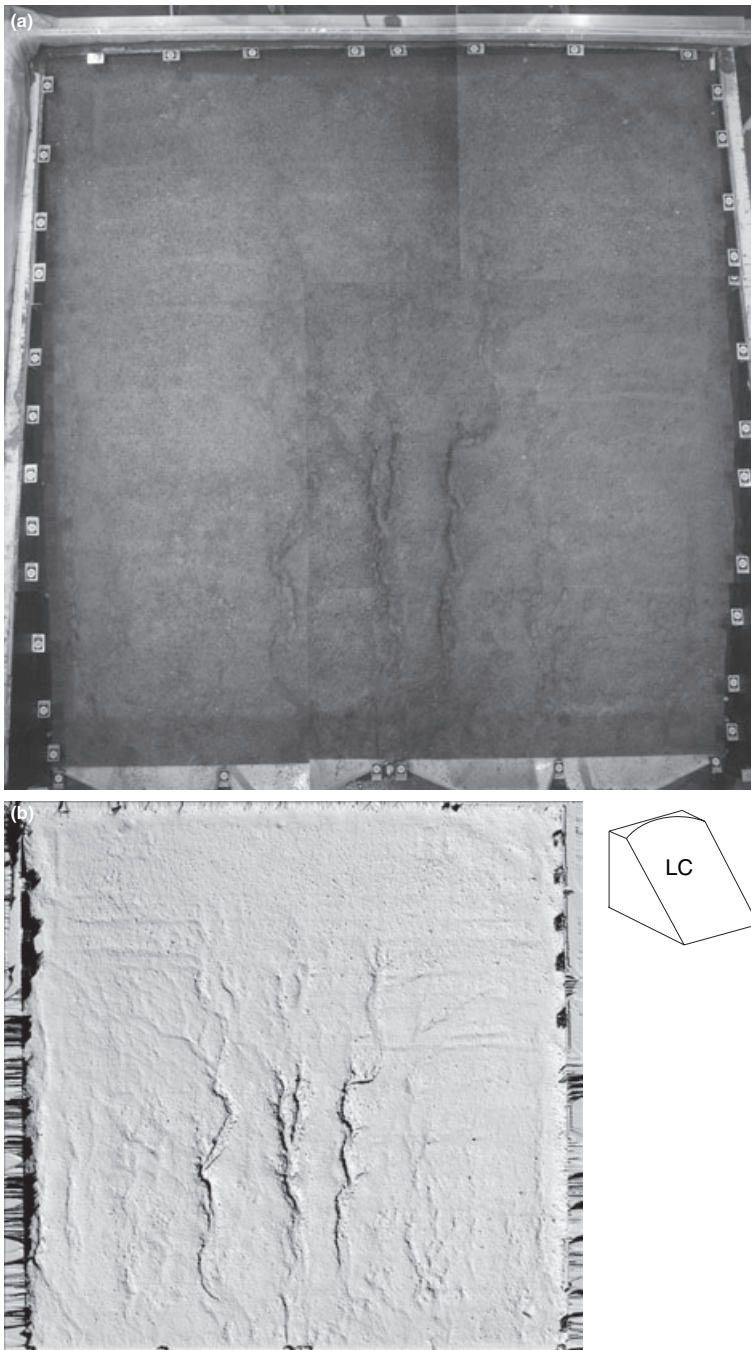


FIG. 5. Mosaic of images (a) after one experiment compared to a hillshading model of the derived DEM from the images (b). A linear convex (LC) slope was prepared for this experiment.

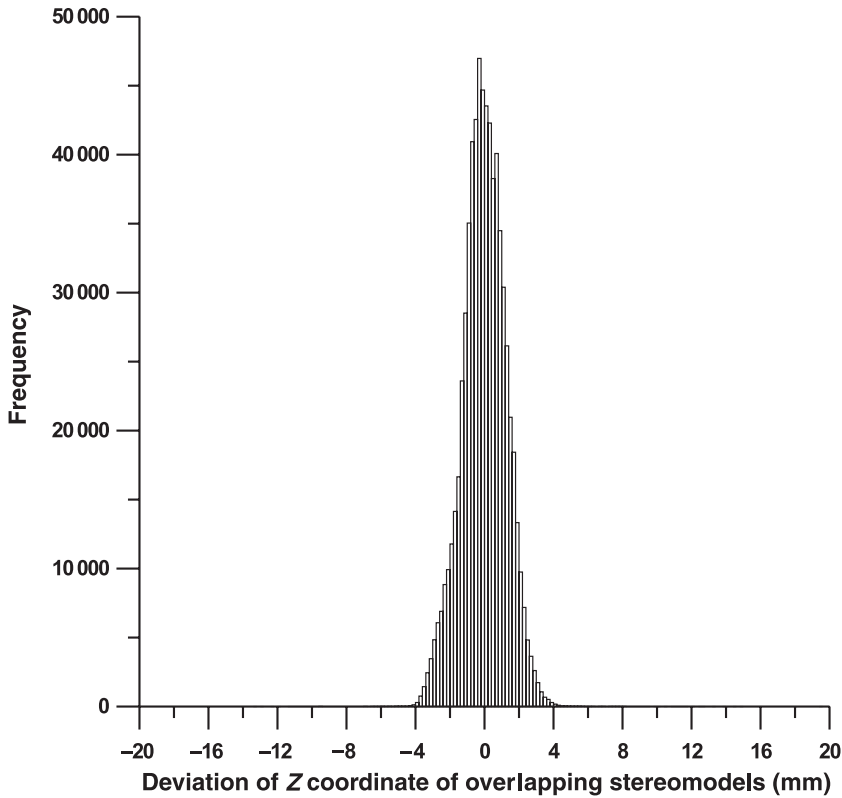
The results of the bundle block adjustment (Tables II and III) suggested sub-millimetre precision for object coordinates. The RMSE of shift parameters of matched image coordinates was approximately 10 times better than  $\sigma_0$  of the bundle block adjustment (Tables II and IV). Therefore, sub-millimetre precision could be expected for object coordinates calculated from homologous points assuming that  $\sigma_0$  and matching precision both reflected the precision of point measurement in image space. Since no control points were placed on the soil surface, the precision of matched coordinates was evaluated by comparing the object coordinates derived from adjacent stereopairs. Working with 60% forward overlap resulted in an overlapping area between two adjacent stereomodels of approximately 20%. Overlapping areas resulting from 30% sidelap were also included in this analysis. Coordinates in the overlapping areas were compared to check for the relative precision between adjacent stereomodels. BLUH software allows a comparison of coordinates based on their  $X$ ,  $Y$  position. Points of two stereomodels that were up to 0.4 mm apart in the  $X$  and  $Y$  directions were assumed to coincide and their  $Z$  value was compared (Fig. 6). The average deviation of  $Z$  values is close to zero and thus shows only negligible bias in the data set (Fig. 6).

This implies that the bundle block adjustment and the production of homologous points in BLUH and DPCOR software resulted in homogenous precision of the data. The standard deviation of elevation differences was used as an estimate for internal precision of the DEMs. The overall precision estimate of 1.26 mm in the vertical satisfies the project requirements, but falls short of a theoretical precision that can be calculated by error propagation (equation (1)). It also does not reach precision estimates of similar studies by Stojic et al. (1998) and Lascelles et al. (2002). Although both of those studies were based on different research objectives at different scales requiring a different photogrammetric as well as experimental setup, the shortfall of the precision in this study was further investigated.

The positional precision ( $\sigma_{X,Y}$ ) and the precision in the direction of the images ( $\sigma_Z$ ) can be estimated from the values provided in Tables I and II

$$\begin{aligned}\sigma_{X,Y} &= m \cdot \sigma_0 = 0.20[\text{mm}] \\ \sigma_Z &= m \cdot \sigma_0 \cdot h \cdot b^{-1} = 0.52[\text{mm}]\end{aligned}\tag{1}$$

where  $m$ ,  $b$ ,  $h$ , and  $\sigma_0$  represent the image scale, base length, camera height, and a posteriori standard deviation of the bundle block adjustment, respectively. The precision of the final product (DEM) deviates significantly from the calculated precision in equation (1). This can be explained in part, but not solely, by the fact that adjacent DEMs only overlap by 20% (forward overlap) to 30% (sidelap). In all these cases coordinates derived from the edges of the image frame were used in the comparison. Success and precision of image matching in these areas can be lower, because of large relief displacement that imposes problems for the software algorithm. Edges of images also show larger residuals in camera calibration, resulting in lower precision for the derived coordinates. Introducing the 1 mm parallax limit for intersection in space significantly reduced these problems. Object coordinates with low precision were removed from the data set. Therefore, most of the remaining discrepancy between theoretical and actual precision must result from more fundamental problems affecting all object coordinates in the model area. The precision estimate of matching in image space was much better (Table IV) than the precision of the bundle block adjustment (Table II), which can be interpreted as the measurement accuracy of the image coordinates. This implies that camera calibration, not matching precision, was the limiting factor of coordinate precision. A study was designed in collaboration with the University of Applied Sciences in Oldenburg, Germany, to test this hypothesis. BLUH software was compared to Rollei (2002) CDW bundle block



<i>Parameter</i>	<i>Value (mm)</i>
Mean elevation difference	-0.02
Standard error of elevation differences	1.26
Maximum positive deviation	19.54
Maximum negative deviation	-13.25
Range	32.79

FIG. 6. Differences in corresponding Z values from object coordinates of overlapping stereomodels based on a sample of 10 overlapping stereomodels. The coordinates from different stereomodels are separated by at most 0.4 mm in the X or Y direction. Data were compared from stereomodels showing the experimental flume after 90 min of rainfall with deep and narrow rills present on the surface. The graph is based on a sample of 691 148 points.

adjustment software that was designed for close range application and employs a different set of additional parameters from BLUH. Twenty-eight images were taken from a testfield with 72 signalled control points. Image coordinates of the targets were measured with a precision of better than 0.02 pixel (Luhmann, 2000). The study revealed that CDW software was capable of producing more accurate results than BLUH from the same data set (Table V).

This implies that the Rollei software is capable of handling the interior geometry of the Kodak DCS 1 m camera with the 19 mm lens better than the BLUH software, which was originally designed for aerial triangulation with large format cameras (Jacobsen, 1980). While

TABLE V. Performance comparison of bundle block adjustment software that uses different sets of additional parameters calibrating the Kodak DCS 1 m camera with the 19 mm lens.

<i>Software</i>	<i>A posteriori <math>\sigma_0</math> (<math>\mu\text{m}</math>)</i>	<i>Precision<sup>a</sup></i>
Rollei CDW	0.35	1:200 000
BLUH	1.65	1:120 000

<sup>a</sup>Precision was calculated as the RMSE of adjusted object coordinates divided by the longest distance in the calibration volume.

this observation might not hold for all types of camera, this comparison indicates that better DEM precision might be reached by modelling the camera parameters in a different way. In addition to that, precision might be increased using different targets as well as different point measurement algorithms. The laminated targets that were used for the experiments here withstood water and dust for months, but were not the best choice when using point measurement operators. The thin plastic covers can shift the location of the centre when looking from different directions. The surfaces of the targets can reflect light, making it impossible to correctly identify the centre in some cases (Fig. 7). In this case, control points were excluded from the bundle block adjustment. Another possible factor affecting the accuracy of target measurement were shadows that partly covered a target (Fig. 7). Errors caused by this effect are difficult to identify from the data set and undoubtedly reduced overall precision of the bundle block adjustment. Therefore, better targets in combination with better target measurement software, and different bundle block adjustment software could significantly increase overall precision of the data.

The region-growing algorithm of DPCOR works best for a close spacing of attempted matches. The algorithm can get lost more easily with increased step sizes that are required for wider grid spacing. Applying epipolar matching or vertical line locus strategies should lead to quicker and more robust results. Software supporting these strategies that were previously not



FIG. 7. Control points were signalled with laminated target points. Laser printouts of concentric black and white circles were laminated to withstand dust and moisture during the experiments. While target 1005 is easily visible in this image that was cropped from Fig. 4, target 2908 shows light reflections, making it impossible to correctly identify the centre of the target with an automated measurement operator. The shadow over target 2908 also affects the centre of gravity algorithm of DPLX. Precise measurements are only possible on well-illuminated targets that were not obstructed or partly shadowed.

available for personal computers are now available on the market, but are still limited in parameter control (ERDAS, 2002; Linder, 2003).

Difference DEMs of the soil surfaces at different stages of the experiment were calculated. The volume removed was compared to the sediment volume collected at the bottom end of the flume. The calculated volumes were larger than the collected sediment yield. This discrepancy can be explained as due to consolidation of the soil that was packed in the box. Such soil settling accounted, on average, for 29% of the calculated sediment yield. Average soil settling for all experiments was 4.2 mm. This effect is often observed in rainfall simulation experiments. For example, Favis-Mortlock (personal communication, 2003) also recognised this effect when comparing flume-end sediment volumes from several rainfall simulation experiments with soil loss volumes calculated from before-and-after DEMs; silt loams and loessial soils were used in these experiments. The effect is not universal, however; Hancock and Willgoose (2001) were able to calculate soil losses that agreed well with the collected sediment yield. Note though that their experimental setup made use of fly ash as an analogue material instead of natural soil.

While the photogrammetric software allowed for control of the important parameters during the process of DEM generation, its low degree of automation made post-processing of data time consuming. The CPU-intensive matching strategy of DPCOR required 1 h for matching one pair of images on a Pentium III personal computer with 1 GHz processor speed. Signalised points as well as tie points had to be measured manually. Automatic tie point generation was not available in DPLX software. At the same time, a bare soil surface does not offer pronounced features that are suitable for automatic tie point generation meaning that manual tie point measurement will be the best solution.

For further analysis of the DEMs, the evolution of the rill network was tracked over time. Rills were calculated from the DEMs using a standard routine in ArcView 3.2a GIS. The calculated rills coincide well with the observed rills in the flume (Fig. 8).

It was shown that rill evolution with time tended towards minimisation of energy expenditure on the soil surface for all slope shapes prepared in this experiment (Rieke-Zapp, 2002). This is a significant scientific result that it was possible to obtain from DEMs taken using photogrammetry due to the quick data acquisition time. Also, no other method would have allowed for the wide vertical range measured here. The generation of DEMs with a resolution of 3 mm and a precision of approximately 1 mm in the vertical was more than sufficient to satisfy the goals of the erosion measurements made in this experiment.

## CONCLUSIONS

Digital close range photogrammetry was used to measure soil surface changes during a laboratory experiment to a level of accuracy of approximately 1 mm. The results allowed for a detailed analysis of the generation of rill networks on complex-shaped surfaces in a short period of time during the experiment. No other currently used method would have satisfied the objectives of the experiment. Adjustments had to be made to the software to optimise results of the DEMs. There was a trade-off between the short periods of time spent on the job and the large amounts of time spent in post-processing the data. Different algorithms could increase the precision of the DEMs and reduce computing time for future projects. Such software is becoming increasingly more available and easy to use on ever faster personal computers.

Mastering different software products originally designed for expert users requires a thorough understanding of the basics of photogrammetry. This results in a significant effort by the soil scientist, but in turn helps the users to optimise their results, be more aware of helpful developments for future applications, and compare the growing number of photogrammetric software packages aimed at the non-photogrammetrist.



FIG. 8. A hillshading model of one soil surface DEM, three times exaggerated in Z. The rill network that developed on the surface was generated from the DEM and overlain on top of the DEM.

In recent high-resolution digital cameras the manufacturers have fixed the sensor in the film plane. There is no need to physically alter the cameras to improve their geometric stability or to use image variant calibration techniques to account for these problems. Today, the design of digital cameras is also more rugged. Cameras are designed for everyday use, and some models are sealed against dust and splashes of water. This is a great improvement when working on rainfall experiments in a soil erosion laboratory.

Soil scientists have made increased use of digital photogrammetry over the past several years. Photogrammetric solutions are competing today with other optical 3D measurement techniques, for example, commercial close range laser scanners and direct 3D measurements using stripe projection systems.

#### ACKNOWLEDGEMENTS

The presented research was undertaken while the authors were affiliated with the National Soil Erosion Research Laboratory and Purdue University in West Lafayette, Indiana, USA. Support by Subaru Isuzu Automotive, Lafayette, Indiana, USA, as well as by Werner Tecklenburg and Heidi Hastedt from the University of Applied Sciences in Oldenburg, Germany, is greatly appreciated. Names of companies mentioned in this text do not imply any preference by the authors or their affiliation with a certain product or brand.

## REFERENCES

- BRASINGTON, J. and SMART, R. M. A., 2003. Close range digital photogrammetric analysis of experimental drainage basin evolution. *Earth Surface Processes and Landforms*, 28(3): 231–247.
- CHANDLER, J., ASHMORE, P., PAOLO, C., GOOCH, M. and VARKARIS, F., 2002. Monitoring river-channel change using terrestrial oblique digital imagery and automated digital photogrammetry. *Annals of the Association of American Geographers*, 92(4): 631–644.
- CLEGG, Z., FARRIS, P. J. and POESEN, J. W., 1999. Soil surface drip point features: an integrated approach using analytical photogrammetry and soil micromorphology. *Catena*, 35(2–4): 303–316.
- DARBOUX, F. and HUANG, C., 2003. An instantaneous-profile laser scanner to measure soil surface microtopography. *Soil Science Society of America Journal*, 67(1): 92–99.
- DPCOR, 2000. *DPCOR user's manual*. Institute of Photogrammetry and Engineering Surveys, University of Hanover, Hanover. 12 pages.
- DPLX, 2000. *DPLX user's manual*. Institute of Photogrammetry and Engineering Surveys, University of Hanover, Hanover. 16 pages.
- ELLIOT, W. J., LAFLIN, J. M., THOMAS, A. W. and KOHL, K. D., 1997. Photogrammetric and rillmeter techniques for hydraulic measurement in soil erosion studies. *Transactions of the American Society of Agricultural Engineers*, 40(1): 157–165.
- ERDAS, 2002. *IMAGINE OrthoBASE user's guide Version 8.6*. Leica Geosystems, Atlanta. 484 pages.
- FAVIS-MORTLOCK, D. T., 1998. A self-organising dynamic systems approach to the simulation of rill initiation and development on hillslopes. *Computers and Geosciences*, 24(4): 353–372.
- FORKERT, G. and STANEK, H., 1997. Der Einsatz der Kodak DCS 460 für die digitale Photogrammetrie. Paper presented at the IX International Geodetic Week, Obergurgl, Austria. 5 pages.
- GODDING, R., 1993. Ein photogrammetrisches Verfahren zur Überprüfung und Kalibrierung digitaler Bildaufnahmesysteme. *Zeitschrift für Photogrammetrie und Fernerkundung*, 61(2): 82–90.
- GRUEN, A., 1985. Adaptive least squares correlation: a powerful image matching technique. *South African Journal of Photogrammetry, Remote Sensing and Cartography*, 14(3): 175–187.
- GRUEN, A., 2001. Least squares matching: a fundamental measurement algorithm. *Close Range Photogrammetry and Machine Vision* (Ed. K. B. Atkinson). Whittles, Caithness. 371 pages: 217–255.
- GRUEN, A., MAAS, H.-G. and KELLER, A., 1995. Kodak DCS200—a camera for high accuracy measurements? *Videometrics IV*, SPIE 2598: 52–59.
- HANCOCK, G. R. and WILLGOOSE, G. R., 2001. The interaction between hydrology and geomorphology in a landscape simulator experiment. *Hydrological Processes*, 15(1): 115–133.
- HUANG, C., 1998. Quantification of soil surface microtopography and surface roughness. *Fractals in Soil Science* (Eds. P. Baveye, J.-Y. Parlange and B. A. Stewart). CRC Press, Boca Raton. 432 pages: 153–168.
- HUANG, C., WHITE, I., THWAITE, E. G. and BENDELI, A., 1988. A noncontact laser system for measuring soil surface topography. *Soil Science Society of America Journal*, 52(2): 350–355.
- JACOBSEN, K., 1980. *Vorschläge zur Konzeption und zur Bearbeitung von Bündelblockausgleichungen*. Ph.D. dissertation, University of Hanover, Hanover, Germany. 142 pages.
- JACOBSEN, K., 2000. *Program System BLUH user's manual*. Institute of Photogrammetry and Engineering Surveys, University of Hanover, Hanover. 444 pages.
- JESCHKE, W., 1990. Digital close-range photogrammetry for surface measurement. *International Archives of Photogrammetry and Remote Sensing*, 28(5): 1058–1065.
- KIRBY, R. P., 1991. Measurement of surface roughness in desert terrain by close range photogrammetry. *Photogrammetric Record*, 13(78): 855–875.
- KUIPERS, H., 1957. A reliefmeter for soil cultivation studies. *Netherlands Journal of Agricultural Science*, 5: 255–262.
- LASCELLES, B., FAVIS-MORTLOCK, D., PARSONS, T. and BOARDMAN, J., 2002. Automated digital photogrammetry: a valuable tool for small-scale geomorphological research for the non-photogrammetrist? *Transactions in GIS*, 6(1): 5–15.
- LINDER, W., 2003. *Digital Photogrammetry—Theory and Applications*. Springer, Heidelberg. 189 pages.
- LUHMANN, T., 2000. *Nahbereichsphotogrammetrie*. Wichmann, Heidelberg. 571 pages.
- MAAS, H.-G., 1999. Ein Ansatz zur Selbstkalibrierung von Kameras mit instabiler innerer Orientierung. *Publikationen der Deutschen Gesellschaft für Photogrammetrie und Fernerkundung*, Band 7 (Eds. J. Albertz and S. W. Dech). Weinert, Berlin. 496 pages: 47–53.
- MEREL, A. P. and FARRIS, P. J., 1998. The monitoring of soil surface development using analytical photogrammetry. *Photogrammetric Record*, 16(92): 331–345.
- OTTO, G. P. and CHAU, T. K. W., 1989. “Region-growing” algorithm for matching of terrain images. *Image and Vision Computing*, 7(2): 83–94.

- PEIPE, J. and SCHNEIDER, C.-T., 2003. CCD oder CMOS—ein Praxisbericht. *Photogrammetrie Fernerkundung Geoinformation*, 7(5): 423–428.
- PYLE, C. J., RICHARDS, K. S. and CHANDLER, J. H., 1997. Digital photogrammetric monitoring of river bank erosion. *Photogrammetric Record*, 15(89): 753–764.
- RIEKE-ZAPP, D. H., 2002. *Digital close range photogrammetry for generation of digital soil surface elevation models—methodology and applications for soil erosion experiments*. Ph.D. dissertation, Purdue University, West Lafayette, Indiana. 204 pages.
- RIEKE-ZAPP, D. H., WEGMANN, H., SANTEL, F. and NEARING, M. A., 2001. Digital photogrammetry for measuring soil surface roughness. *Proceedings of the American Society of Photogrammetry & Remote Sensing 2001 Conference: Gateway to the New Millennium*, St Louis, Missouri. 8 pages.
- ROLLEI, 2002. *Close range digital workstation user's manual Version 2.1*. Rollei, Braunschweig. 235 pages.
- RÖMKENS, M. J. M., SINGARAYAR, S. and GANTZER, C. J., 1986. An automated non-contact surface profile meter. *Soil and Tillage Research*, 6(2): 193–202.
- STOJIC, M., CHANDLER, J., ASHMORE, P. and LUCE, J., 1998. The assessment of sediment transport rates by automated digital photogrammetry. *Photogrammetric Engineering & Remote Sensing*, 64(5): 387–395.
- TECKLENBURG, W. and LUHMANN, T., 2001. Kameramodellierung mit bildvarianten Parametern und Finiten Elementen. *Publikationen der Deutschen Gesellschaft für Photogrammetrie und Fernerkundung*, Band 9 (Ed. J. Albertz). Weinert, Berlin. 409 pages: 140–149.
- WEGMANN, H., RIEKE-ZAPP, D. and SANTEL, F., 2001. Digitale Nahbereichsphotogrammetrie zur Erstellung von Oberflächenmodellen für Bodenerosionsversuche. *Publikationen der Deutschen Gesellschaft für Photogrammetrie und Fernerkundung*, Band 9 (Ed. J. Albertz). Weinert, Berlin. 409 pages: 165–173.
- WELCH, R. and JORDAN, T. R., 1983. Analytical non-metric close-range photogrammetry for monitoring stream channel erosion. *Photogrammetric Engineering & Remote Sensing*, 49(3): 367–374.
- WESTER-EBBINGHAUS, W., 1985. Verfahren zur Feldkalibrierung von photogrammetrischen Aufnahmesystemen im Nahbereich. *Kammerkalibrierung in der photogrammetrischen Praxis* (Eds. G. Kupfer and W. Wester-Ebbinghaus). Deutsche Geodätische Kommission, Reihe B, Nr. 275, Beck, Munich. 181 pages: 106–114.

### Résumé

*De nombreux phénomènes impliqués dans l'érosion des sols ont des dimensions à l'échelle du millimètre. Leur quantification et leur modélisation nécessitent des informations sur la surface topographique de ces terrains avec des résolutions bien adaptées. L'objectif de cette étude était l'établissement de modèles numériques des altitudes (MNA) de la surface du sol avec de grandes résolutions spatiales et temporelles. On a utilisé la photogrammétrie numérique pour déterminer les taux d'érosion de sols de formes complexes soumis à des précipitations en laboratoire. On a en tout réalisé 60 MNA couvrant en planimétrie une superficie de 16 m<sup>2</sup>, avec une résolution de grille de 3 mm. La précision altimétrique souhaitée était d'environ 1 mm, de façon à pouvoir bien analyser ces MNA. On a utilisé une caméra numérique courante pour l'acquisition des images. On a étalonné la caméra avec le logiciel BLUH. On a identifié les points homologues des images en recouvrement stéréoscopique avec un logiciel d'appariement par moindres carrés. On a établi une grille régulière dans un système d'informations géographique en interpolant les coordonnées-objet de points irrégulièrement espacés. Les MNA résultants représentaient correctement la surface des sols. On est arrivé à une précision altimétrique de 1.26 mm. C'est l'étalonnage de la caméra qui a limité la précision des MNA obtenus. Parmi les améliorations souhaitables du système on peut mentionner l'emploi de meilleurs points d'appui et des stratégies d'appariement d'images plus élaborées pour l'identification des points homologues. Ces MNA ont permis des analyses détaillées de l'évolution de la surface des sols.*

### Zusammenfassung

Viele Prozesse im Bereich der Bodenerosionsforschung spielen sich im Millimeter-Maßstab ab. Für die Modellierung und Quantifizierung solcher Prozesse werden Informationen mit adäquater Auflösung benötigt. Die Aufgabe dieser Arbeit bestand darin, Digitale Höhenmodelle (DHM) mit hoher räumlicher und zeitlicher Auflösung zu erstellen, um Erosionsraten auf komplex geformten Versuchsfächen während Regensimulationsversuchen im Labor zu messen. Insgesamt wurden 60 Höhenmodelle mit einer Gitterauflösung von 3 mm von einer 16 m<sup>2</sup> großen Versuchsfäche erzeugt. Für die Höhenmodelle wurde eine Höhengenaugigkeit von 1 mm angestrebt. Für die Aufnahmen wurde eine digitale Amateurkamera verwendet und mit der BLUH Software kalibriert. Homologe Punkte in überlappenden Bildern wurden mit einem Bildzuordnungsverfahren nach der Methode der Kleinsten Quadrate identifiziert. Unregelmäßig im Raum verteilte Objektkoordinaten wurden in einem Geographischen Informationssystem zu regelmäßigen Gittern interpoliert. Die Bodenoberflächen wurden von den Digitalen Höhenmodellen gut wiedergegeben. Es wurde eine Höhengenaugigkeit von 1.26 mm erreicht. Limitierender Faktor für die Genauigkeit war die Kamerakalibrierung. Die Verwendung geeigneterer Passpunkte sowie fortschrittlicherer Bildzuordnungsstrategien zur Identifikation homologer Punkte könnten das bestehende System weiter verbessern. Die erzeugten Höhenmodelle erlaubten eine detaillierte Analyse der Bodenoberflächenentwicklung.

### Resumen

Muchos de los procesos involucrados en erosión de suelos se encuentran en el rango de escala milimétrica. El modelamiento y cuantificación de dichos procesos requieren tanto de una precisa información de suelos como de una adecuada resolución de la superficie topográfica. El motivo de este estudio es la generación de Modelos Digitales de Terreno (MDT) a partir de superficies de suelos con una alta resolución espacial y baja resolución temporal. Bajo condiciones de lluvia controlada en laboratorio, fotogrametría digital fue utilizada para la evaluación de velocidades de erosión en superficies complejas de suelos. Un total de 60 MDT fueron generados, cubriendo una superficie total planimétrica de 16 m<sup>2</sup> con una resolución espacial de 3 mm. Para el análisis de los MDT, fue deseada una precisión vertical aproximada de 1 mm. Para la adquisición de las imágenes digitales fue utilizada una cámara de consumo masivo, calibrada usando el programa computacional BLUH. Puntos homólogos en las áreas de traslape de imágenes fueron identificados con un programa computacional usando mínimos cuadrados. Objetos con coordenadas espaciadas irregularmente fueron interpolados a una grilla regular en un sistema de información geográfico. Los MDT resultantes entregaron una fiel representación de la superficie de suelos con una precisión vertical de 1.26 mm, esta última, directamente ligada a la calibración de la cámara utilizada. Mejoramientos en la configuración incluirían el uso de mejores puntos de control y más avanzadas estrategias de correlación para la identificación de puntos homólogos en las imágenes. Los MDT generados permitieron un análisis detallado de la evolución de la superficie del suelo.